Monitoring Solvent Evaporation from Thin Films by Localized Surface Plasmon Resonance Shifts

ARTICLE *in* THE JOURNAL OF PHYSICAL CHEMISTRY C · OCTOBER 2010

Impact Factor: 4.77 · DOI: 10.1021/jp106528n

2 AUTHORS, INCLUDING:

Paula C. Angelomé
Comisión Nacional de Energía Atómica
24 PUBLICATIONS **686** CITATIONS

Monitoring Solvent Evaporation from Thin Films by Localized Surface Plasmon Resonance Shifts

Paula C. Angelomé* and Luis M. Liz-Marzán

Departamento de Química Física and Unidad Asociada CSIC-Universidade de Vigo, 36310 Vigo, Spain

Received: July 14, 2010; Revised Manuscript Received: September 17, 2010

In this work, new composite materials consisting of a submonolayer of metallic nanoparticles (spheres or decahedra) chemically bound to a glass slide and covered with a sol−gel thin film (with or without templating) were synthesized. Nanoparticles can be fully covered by well-ordered mesoporous thin films, when templated films are synthesized. The particles underneath the porous films remain accessible but not in direct contact with the outer medium, and their plasmon band shifts with changes in the refractive index of the solvent that wets the film. Taking advantage of this phenomenon, we monitored the evaporation of solvents through changes in the plasmon band position for various thin films and solvents, using UV−visible spectroscopy. This procedure can be generalized to different metal particles, thin films, and solvents, thus paving the way toward new composite materials containing an active layer of metallic particles that can be used to investigate the interactions between solvents and oxide thin films.

Introduction

The attractive optical properties of metal nanostructures are connected to their localized surface plasmon resonance (LSPR). The LSPR is an optical phenomenon generated by collective oscillations of the electron gas in metal nanostructures surrounded by a dielectric.[1] The LSPR spectral position is highly dependent on the composition, size, or shape of the nanoparticles, as well as on the refractive index of the medium around them.[2] Therefore, changes in the dielectric environment around metallic nanoparticles can be monitored via LSPR peak shifts, with different performance according to the type of particles. In particular, the red shift induced by a refractive index increase around metal nanostructures is the basis of the so-called refractive index sensors, which are widely used for biological applications.[3,4] Noble metals, especially silver and gold, are typically chosen for these analytical purposes. Although silver displays better optical properties than gold, the higher chemical stability of gold nanostructures has favored their preferential application.

When metal nanostructures interact with a light beam, some of the incident photons are absorbed, while others are scattered. Both absorption and scattering are greatly enhanced when the LSPR is excited. Consequently, spectroscopy is the simplest method to detect the LSPR on metal nanostructures or in low absorption materials containing nanoparticles (nanocomposites). If the system contains a large amount of nanoparticles, UV−visible spectroscopy is a reliable and simple technique to determine changes in the LSPR position. Although many reports have been published on the use of metallic nanoparticles to sense biological or chemical reactions,[3,4] the application of refractive index sensing to monitor physical processes such as solvent evaporation or other reversible changes in the particles' environment is far less frequent.

On the other hand, the synthesis of mesoporous materials has experienced an explosive growth during the last 15 years. These materials are formed by using micellar and lyotropic liquid-crystal phases as templates, allowing one to obtain high specific surface area materials with highly ordered arrays of monodisperse pores. The field started its development with the M41S silica family, but an increasing amount of mesoporous materials with very diverse chemical compositions (oxides, metals, carbons, semiconductors, etc.), shaped as powders, monoliths, thin films, membranes, or fibers, was later developed.[5,6] Oxide thin films such as mesoporous SiO_2 or TiO_2 are particularly interesting due to their possible applications in diverse fields such as (bio)sensing, catalysis, adsorption, separation, drug delivery, optical devices, etc. However, thin films also represent a challenge to traditional characterization techniques because they are made of a very small amount of material (up to 500 $\mu g/cm^2$ of film) on top of a bulk substrate. These properties make their characterization more difficult than in the case of bulk materials and limit the techniques that can be used.[5] In particular, the study of the interaction between solvents and mesoporous materials requires specific techniques that can detect small changes in the properties of the thin film during its contact with the solvent. For this purpose, ellipsometric porosimetry has been developed,[7−10] and X-ray reflectivity[11−13] was adapted. In both cases, dedicated equipment is required to perform the measurements.

Several examples have been reported regarding the combination of mesoporous oxide thin films with metallic nanoparticles[14−16] mainly for catalysis, biosensing, and nonlinear optics applications. The final composites are typically obtained by means of four main methodologies: (a) including preformed nanoparticles during the synthesis of the sol−gel material, (b) synthesizing the oxide and the nanoparticles at the same time, (c) synthesizing the metal inside the preformed oxide, and (d) incorporating the nanoparticles inside the preformed oxide.[15] The availability for chemical reactions of particles included within oxide films has also been studied with successful results. For example, Hu et al. studied the changes in the LSPR of Ag nanoparticles included in a mesoporous SiO_2 thin film due to the exposure to different atmospheres.[17] Also, Bois et al. studied the color changes produced due to oxidation in Ag particles

* To whom correspondence should be addressed. E-mail: angelome@uvigo.es.

10.1021/jp106528n
Published on Web 10/07/2010

grown inside mesoporous TiO_2.[18] Once again, no physical processes were studied in this type of composite materials.

In this work, new composite materials consisting of a submonolayer of metallic nanoparticles (spheres or decahedra) chemically bound to a glass slide and covered with a sol−gel thin film (with or without templating) were synthesized. The method leads to formation of fully covered metallic particles and well-ordered mesoporous thin films. The particles underneath the porous films remain accessible but not in direct contact with the medium, and the LSPR band changes its position as a function of the refractive index of the solvent wetting the film. Taking advantage of this phenomenon, solvent evaporation was monitored by registering the changes in the LSPR band position for various thin films and solvents. As the whole procedure can be repeated with different metallic particles, thin films, and solvents, these composite materials can be used to follow interactions between the solvents and the thin film deposited on the top of the metal nanoparticles, using a rather simple measurement technique such as UV−visible spectroscopy. These results are expected to complement and help to understand previous reports on solvent−mesoporous material interaction, based on the use of more complex techniques.

Experimental Section

Materials. $HAuCl_4 \cdot 3H_2O$, trisodium citrate dihydrate, $NaBH_4$, HCl(c), tetraethoxysilane (TEOS), $TiCl_4$, 3-aminopropyltrimethoxysilane (APS), 3-mercaptopropyltrimethoxysilane (MPS), H_2O_2 (28%), 1-propanol, and sulfuric acid (98%) were supplied by Aldrich. The triblock copolymer Pluronic F127 $[HO(CH_2CH_2O)_{106}(CH_2CH(CH_3)O)_{70}\text{-}(CH_2CH_2O)_{106}OH]$ was purchased from Sigma. Poly(vinylpyrrolidone) (PVP, average molecular weight 10000 g mol^{-1}) and *N*,*N*-dimethylformamide (DMF) were supplied by Fluka. Dry toluene was supplied by Scharlab. All chemicals were used as received. Pure grade ethanol, acetone, and Milli-Q grade water were used as solvents.

Particle Preparation. Gold nanodecahedra (44 nm side length) were prepared according to a procedure previously reported[19] and were purified by several centrifugation−redispersion cycles, using ethanol as the solvent. Gold spheres (15 nm diameter) were synthesized by the Turkevich method[20] and used without further purification.

Glass Preparation. Glass slides were cleaned with piranha solution (3 H_2SO_4:1 H_2O_2) for at least 30 min, then copiously rinsed with pure water, and kept under water until use. Dry glass slides were immersed in a 0.01 M (in ethanol) solution of APS for 3 h or MPS for 1 h, rinsed with ethanol, and then immersed for variable time in Au nanoparticles solution. APS-modified glass slides were used for sphere attachment, whereas MPS-modified slides were selected for decahedra.

Preparation of Mesoporous Films. Titania and silica mesoporous thin films were produced by spin coating on top of the gold nanoparticle modified glasses, at a spinning rate of 4000 rpm and using 125 μL of solution. The detailed preparation techniques of the sols have been reported elsewhere.[21,22] Initial silica solutions were composed of TEOS/EtOH/F127/H_2O/HCl mixture, with a 1:40:0.005:10:0.008 ratio of the reagents. These solutions were aged for 72 h at room temperature prior to utilization. The titania solution was composed of $TiCl_4$/EtOH/F127/H_2O with a ratio of 1:40:0.005:10 and used fresh (no aging). The use of Pluronic F127 as template allows one to obtain mesoporous thin films with pores ordered in a body-centered cubic face (*Im3m*), with an interpore distance of about 12 nm.[21] Nontemplated oxides were synthesized using the same procedure but without addition of Pluronic F127 to the initial solution. After spin coating, the films were placed in 50% relative humidity chambers (obtained with a NaBr-saturated solution) for 24 h and subjected to a stabilizing thermal treatment comprising two successive 24 h heat treatments at 60 and 120 °C and a final 2 h step at 200 °C. The template was then removed by immersing the films for 3 days in ethanol.

Materials Characterization. UV−visible spectra were recorded using an Agilent 8453 UV−visible spectrophotometer. Transmission electron microscopy (TEM) analysis was performed with a JEOL JEM1010 microscope operating at an acceleration voltage of 100 kV. Samples for TEM were obtained by scratching the films from the substrate and depositing them on carbon and FORMVAR-coated copper grids.

X-ray photoelectron spectroscopy (XPS) analysis of the samples was performed using a Thermo Scientific K-Alpha ESCA instrument. Because of the nonconductor nature of the samples, it was necessary to use an electron flood gun to minimize surface charging. Neutralization of the surface charge was performed by using both a low-energy flood gun (electrons in the range of 0−14 eV) and a low-energy Ar ion gun. The measurements were carried out using monochromatic Al−K radiation (1486.6 eV).

Solvent Evaporation Measurements. A quartz cuvette (1 cm optical path length) containing the solid sample was introduced inside the thermostatted (80 °C) sample holder of the UV−vis spectrophotometer. The cuvette was then filled with the appropriate solvent and allowed to stabilize for several minutes, the solvent was removed, and data collection was started. The evaporation process was followed by recording spectra (350−1100 nm range) every 30 s for 30 min. A clean glass slide inside a similar cuvette was used as the blank.

Results and Discussion

The main objective of this work was to demonstrate the applicability of gold nanoparticles to characterize the porosity of thin films in general and of mesoporous oxides in particular. The characterization is based on the refractive index sensitivity of surface plasmon resonances in nanometals and thus comprises monitoring over time the UV−visible spectra of the films, covering a uniform distribution of gold nanoparticles.

The main preparation procedure thus comprised the deposition of gold nanoparticles onto glass surfaces, followed by coverage with sol−gel thin films of various types. The coverage step was carried out by spin coating and post-treatment of the obtained thin films, as typically used for pure glass substrates. Although mesoporous thin films have been successfully prepared using different conditions and substrates,[5] the presence of the particles chemically attached on top of the substrate could alter the process, and thus, it was necessary to carry out a detailed characterization to ensure that mesoporous film formation and particle position on the glass were not affected.

Direct evidence about the morphology and mesostructure of the system can be obtained through TEM observation. Because of the nature of the technique, the specimens were prepared by scratching the composite thin films and depositing small pieces on carbon-coated grids (note that scratching might induce some damage). In all cases, TEM observation revealed no meaningful differences between the films prepared on pure glass slides and those containing gold nanoparticles. Representative images are shown in Figure 1a,b, for TiO_2 and SiO_2 mesoporous thin films formed on top of gold nanodecahedra. First of all, it was observed that the nanoparticles are randomly dispersed in the film, with no significant aggregation. Additionally, the porous pattern follows that expected for the *Im3m* cubic phase with

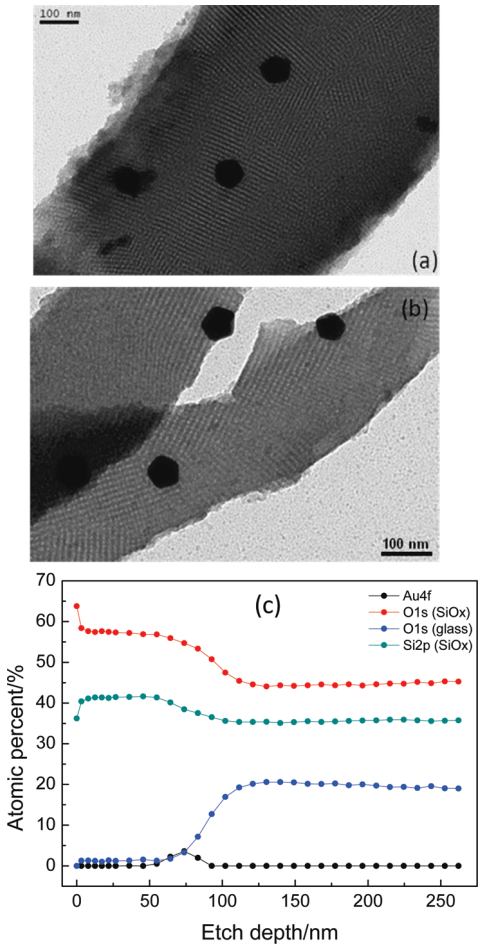

Figure 1. Representative TEM images of scratched samples: (a) Au decahedra covered with TiO_2−F127 mesoporous film, (b) Au decahedra covered with SiO_2−F127 mesoporous film, and (c) XPS elemental depth profile for Au spheres covered with SiO_2−F127 mesoporous film, showing the localization of Au particles.

[110] planes oriented parallel to the substrate, which is the phase commonly obtained when using Pluronic F127 as a template.[21] This demonstrates that the formation of the mesoporous thin film is not affected by the roughness (at nanoscopic level) of the substrate.

The adsorption of the gold nanoparticles on glass substrates was achieved by chemical bonding (amino-Au or mercapto-Au) upon silanization. Although this was expected to strongly retain the particles, the thin films were prepared via spin coating; therefore, it was necessary to confirm that the particles remain in contact with the glass support upon film formation. XPS depth profile measurements were used for this purpose, because this technique allows us to obtain the elemental distribution through the complete film thickness. Representative results for the case of Au spheres covered with a SiO_2 mesoporous thin film are shown in Figure 1c. It can be clearly seen that the Au 4f signal only starts to develop when a depth of 50 nm is reached, returning back to zero at 90 nm. Additionally, the region in which Au is detected matches with that where a signal typical for glass (O 1s) is detected, indicating that the Au particles are mainly located at the interface between the glass support and the thin film. These experiments ensure that the particles are not in contact with air and have remained around their original positions. We have also noticed that the shape of the LSPR band in the UV−visible spectra (see Figure S1 in the Supporting Information) of the particles before and after film deposition

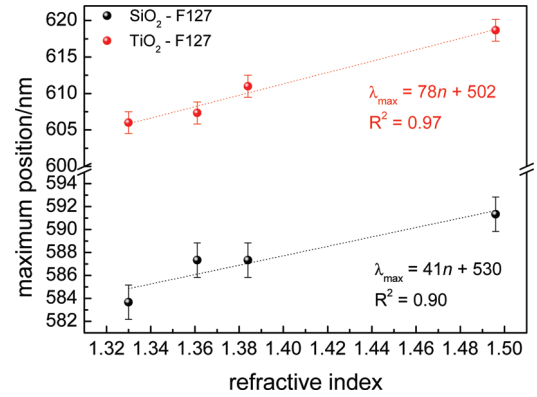

Figure 2. Plasmon band maximum positions for Au decahedra covered with TiO_2 and SiO_2 mesoporous films and immersed in solvents with different refractive indexes.

was not altered, indicating that no aggregation or reshaping occurred during the process. The maximum position, however, was red-shifted, because of the increase in refractive index around the particles, which varied from $n = 1$ (air) up to either ≈1.6−1.7 (for porous TiO_2)[9] or ≈1.2−1.3 (for porous SiO_2).[23]

It has been repeatedly shown[24−26] that the optical spectra (LSPR band) of metal nanoparticles adsorbed on glass substrates are sensitive to changes in the refractive index of the solvent in which they are immersed, and a systematic study has been reported for Au decahedra similar to those used for this work.[27] This sensitivity can be readily determined by monitoring the position of the LSPR band through simple UV−visible spectroscopy measurements. When the gold nanoparticles are covered with mesoporous thin films, which leave a large amount of open space, the same effect is expected to occur. We therefore characterized our Au decahedra−mesoporous film composites by immersing them in various solvents with different refractive indexes and registering their corresponding UV−visible spectra. Between two consecutive immersions, the samples were dried at 120 °C, to ensure that the pores were empty prior to the following measurement.

The variation of the maximum position of the LSPR band as a function of solvent refractive index is shown in Figure 2, for gold decahedra covered with porous TiO_2 and SiO_2 films. As expected, a linear correlation between λ_{max} and solvent refractive index was obtained. However, it should be taken into account that the refractive index in which the particles are immersed is more complex, because they are in contact with the glass substrate and covered by the porous oxide containing the solvent that wets the pores. Because during these experiments only the immersion solvent was varied, the sensitivity toward refractive index changes was expected to be lower than in the case of noncovered particles (i.e., particles attached to a glass and immersed in the solvent). Indeed, this is what we observed: For Au decahedra covered with mesoporous TiO_2, the slope was determined to be 78 nm/refractive index unit (RIU), while for the same particles covered with mesoporous SiO_2, the slope was 41 nm/RIU, and for the bare particles on glass (Figure S2 in the Supporting Information), the slope was around 140 nm/RIU. The same trend was observed in the case of Au spheres (d = 15 nm) covered with SiO_2 porous films (see one example in Figure S3 in the Supporting Information), but the slopes were consistently lower, indicating that these particles are less sensitive to refractive index changes. The difference in the sensitivity between the samples covered with TiO_2 and SiO_2 can be attributed to the different film porosity, which makes the particles deposited underneath more or less accessible to the solvent.

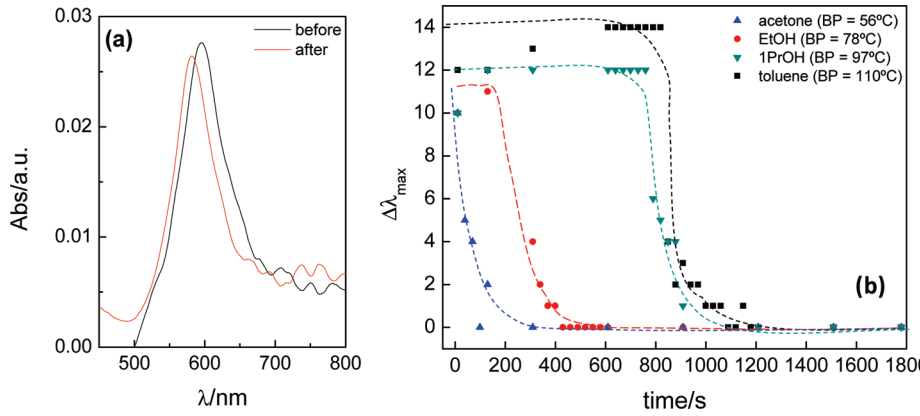

Figure 3. (a) Spectra of Au decahedra covered with a SiO_2−F127 film before (black curve) and after (red curve) toluene evaporation. (b) $\Delta\lambda_{max}$ as a function of time for Au decahedra covered with SiO_2−F127 during the evaporation of different solvents (cell temperature = 80 °C). Lines are guides for the eye.

As a direct consequence of these results and the general nature of the process with regard to the nature of the oxide film and the composition of the solvents, the refractive index sensitivity of these composite materials can be exploited to investigate the interaction between solvents and oxides. As a proof of concept, we show here the results from two different experiments: a study of the evaporation of different solvents from the same oxide film and a study of the evaporation of the same solvent from different oxides, always deposited on top of Au nanodecahedra. These particles were selected because they are highly sensitive to refractive index changes in their immediate environment[27] (see Figure 2).

Evaporation of Different Solvents from Mesoporous SiO_2−F127. For this experiment, glass-supported Au decahedra covered with mesoporous SiO_2−F127 thin films where immersed in different organic solvents (acetone, 1-propanol, ethanol, and toluene), the solvent was removed, and immediately thereafter, UV−vis spectra were recorded as a function of time, using a thermostatted holder to keep the system at 80 °C. As the solvent that remained adsorbed within the porous film was evaporated, a shift of the plasmon band toward lower wavelengths was observed (Figure 3). Once the solvent was completely evaporated, no further changes in the plasmon band position were observed. In fact, the final position of the LSPR band was coincident with that of the dry composite film after treatment in the oven at 120 °C, indicating that no solvent remained inside the pores. In the spectra shown in Figure 3a, one can see that the shift is perfectly consistent with refractive index changes (red shift and increased intensity for higher index), while the kinetic traces in Figure 3b for the variation in plasmon band position as a function of time during solvent evaporation show that the nature of the solvent plays an important role in the way evaporation takes place.

Nevertheless, the solvent evaporation follows the same trend for all solvents and can be divided in three steps: (1) The plasmon position remains constant for a certain time that depends on the solvent, (2) the plasmon band quickly starts to shift toward lower wavelengths, and (3) the band position remains constant again. This indicates that the evaporation of solvents from the interior of mesopores is rapidly completed after it starts, but there is a certain induction period. This behavior was actually expected, on the basis of previous results obtained using either ellipsometric porosimetry[7,8] or X-ray reflectivity,[11,12] regarding the condensation of solvents (in particular, water) inside mesoporous thin films. In those experiments, the capillary condensation inside the pores occurs

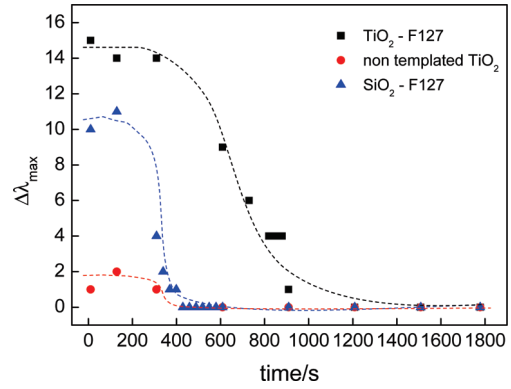

Figure 4. $\Delta\lambda_{max}$ as a function of time for Au decahedra covered with different sol−gel thin films, during the evaporation of ethanol (cell temperature, 80 °C). Lines are guides for the eye.

quickly once a certain vapor pressure (which depends on the type of oxide and its pore size) is reached. The same was observed to occur with solvent elimination as the pressure was lowered, a process that is directly related to evaporation.

When different solvents are compared, all the curves present the same shape but with noticeable differences regarding the duration of the first stage, which seems to be closely related to the respective boiling points of the solvents. In fact, whereas for toluene (boiling point, 110 °C) the first stage takes about 900 s to be completed, it takes less than 10 s for acetone (boiling point, 56 °C). This means that solvents with higher boiling points stay longer inside the porous material, keeping the environment around the particles unchanged, so that the position of the plasmon band does not change either. These results show that with this type of composite materials, it is possible to follow the evaporation rate of different solvents from thin oxide films and to differentiate between solvents, according to their boiling points. However, the interactions between solvent and film are also expected to influence the evaporation conditions.

Evaporation of Ethanol from Different Oxide Films. Au decahedra covered with different sol−gel thin films (mesoporous SiO_2, mesoporous TiO_2, and nontemplated TiO_2) were immersed in ethanol, then the solvent was extracted, and the LSPR band of the particles was then immediately monitored as a function of time at 80 °C. The obtained results were plotted in Figure 4. As in the previous example, as the ethanol that was retained within the porous film evaporates, a blue shift of the plasmon band was observed. For these experiments, it can be observed that the evaporation of the same solvent clearly depends on the nature of the thin film that has been deposited on top of the

particles. Several factors should be taken into account to explain the observed differences: specific interactions between the oxide and the solvent, porosity, and accessibility of the films. In the case of nontemplated TiO_2, not much porosity is available to be filled with the solvent, so the amount of solvent that can actually get in contact with the nanoparticles is significantly lower (2 nm shift in the plasmon band position), and it evaporates faster (completed in ca. 300 s) than in the case of templated oxides.

On the other hand, the difference between porous TiO_2 and porous SiO_2 can be, at least partially, attributed to specific interactions between the solvent and the oxide walls. According to the experimental profiles, the evaporation of ethanol takes longer in TiO_2 (around 700 s) than in SiO_2 (around 350 s), indicating a stronger affinity between the titania walls and ethanol. The interaction of ethanol with SiO_2 is expected to be weaker than in the TiO_2 case, as the availability for reaction and complexation of the Si(IV) center is lower than that of the Ti(IV) center. In fact, the affinity between alcohols and TiO_2 has been previously exploited when using crystalline TiO_2 as a catalyst for ethanol decomposition.[28,29] In the catalysis case, the O−H bond of the alcohol dissociates right upon adsorption. Because in our case crystalline titania was not present, the interaction should not be so strong, but it surely exists.

In the case of toluene evaporation, the difference between porous TiO_2 and SiO_2 is not as marked as in the ethanol case: The evaporation occurs at around 800 s over SiO_2 and around 1000 s over TiO_2 (Figure S4 in the Supporting Information). As toluene is not a polar solvent and cannot complex metallic centers, less specific interactions are expected. In this case, the observed differences could be mainly attributed to thickness and porosity changes between the different films. According to these results, the main conclusion that we can extract is that it is possible to compare different oxides according to their affinity to a certain solvent. This type of measurements could be used, for example, to determine if a film has open porosity or if a reaction that opens or closes the pores of a film has been successful.

Conclusions

A new family of composite materials comprising a submonolayer of metal nanoparticles deposited onto a glass substrate and covered with a sol−gel thin film was devised and synthesized. It was found that the particles remain at the glass/thin film interface, and when the film was templated with a surfactant, well-ordered mesopores were obtained. The particles underneath the oxide film remain accessible to solvents, and their LSPR band can be shifted to different positions according to the refractive index of the solvent wetting the pores. Additionally, the evaporation of the adsorbed solvent can be monitored by simply measuring the plasmon band position as a function of time. The evaporation profile is then related with the boiling point of the solvent, the film type, and its accessibility. As this procedure can be repeated with different metallic particles, thin films, and solvents, we demonstrated the possibility to build new composite materials containing an active layer of metallic particles that can be used to follow the interactions between a solvent and an oxide thin film.

Acknowledgment. This work has been funded by the MiCInn/FEDER (MAT2007-62696) and the Xunta de Galicia (09TMT011314PR). Carmen Serra (CACTI, Univ. Vigo) is thanked for carrying out the XPS measurements and analysis, and Ana Sánchez-Iglesias is thanked for synthesizing Au nanodecahedra.

Supporting Information Available: UV−visible spectra of gold decahedra covered and uncovered with mesoporous thin films; LSPR band maximum position as a function of solvent refractive index for uncovered Au decahedra and SiO_2 covered Au spheres and $\Delta\lambda_{max}$ during the evaporation of toluene for Au decahedra covered with different sol−gel thin films. This material is available free of charge via the Internet at http://pubs.acs.org.

References and Notes

(1) Bohren, C. F.; Huffman, D. R. *Absorption and Scattering by Small Particles*; Wiley-Interscience: New York, 1983.
(2) Liz-Marzan, L. M. *Langmuir* **2006**, *22*, 32.
(3) Sepúlveda, B.; Angelomé, P. C.; Lechuga, L. M.; Liz Marzán, L. M. *Nano Today* **2009**, *4*, 244.
(4) Stewart, M. E.; Anderton, C. R.; Thompson, L. B.; Maria, J.; Gray, S. K.; Nuzzo, R. G. *Chem. Rev.* **2008**, *108*, 494.
(5) Sanchez, C.; Boissière, C.; Grosso, D.; Laberty, C.; Nicole, L. *Chem. Mater.* **2008**, *20*, 682.
(6) Soler-Illia, G. J. d. A. A.; Sanchez, C.; Lebeau, B.; Patarin, J. *Chem. Rev.* **2002**, *102*, 4093.
(7) Boissiere, C.; Grosso, D.; Lepoutre, S.; Nicole, L.; Bruneau, A. B.; Sanchez, C. *Langmuir* **2005**, *21*, 12362.
(8) Fuertes, M. C.; Colodrero, S.; Lozano, G.; Gonzalez-Elipe, A. R.; Grosso, D.; Boissiere, C.; Sanchez, C.; Soler-Illia, G. J. d. A. A.; Miguez, H. *J. Phys. Chem. C* **2008**, *112*, 3157.
(9) Bass, J. D.; Grosso, D.; Boissiere, C.; Sanchez, C. *J. Am. Chem. Soc.* **2008**, *130*, 7882.
(10) May, R. A.; Patel, M. N.; Johnston, K. P.; Stevenson, K. J. *Langmuir* **2009**, *25*, 4498.
(11) Gibaud, A.; Dourdain, S.; Vignaud, G. *Appl. Surf. Sci.* **2006**, *253*, 3.
(12) Yan, M.; Dourdain, S.; Gibaud, A. *Thin Solid Films* **2008**, *516*, 7955.
(13) Klotz, M.; Rouessac, V.; Rébiscoul, D.; Ayral, A.; van der Lee, A. *Thin Solid Films* **2006**, *495*, 214.
(14) Sun, J.; Bao, X. *Chem.—Eur. J.* **2008**, *14*, 7478.
(15) Walters, G.; Parkin, I. P. *J. Mater. Chem.* **2009**, *19*, 574.
(16) White, R. J.; Luque, R.; Budarin, V. L.; Clark, J. H.; Macquarrie, D. J. *Chem. Soc. Rev.* **2009**, *38*, 481.
(17) Hu, J.; Wang, L.; Cai, W.; Li, Y.; Zeng, H.; Zhao, L.; Liu, P. *J. Phys. Chem. C* **2009**, *113*, 19039.
(18) Bois, L.; Chassagneux, F.; Battie, Y.; Bessueille, F. o.; Mollet, L.; Parola, S. p.; Destouches, N.; Toulhoat, N.; Moncoffre, N. *Langmuir* **2009**, *26*, 1199.
(19) Sánchez-Iglesias, A.; Pastoriza-Santos, I.; Pérez Juste, J.; Rodríguez-González, B.; García de Abajo, F. J.; Liz Marzán, L. M. *Adv. Mater.* **2006**, *18*, 2529.
(20) Turkevitch, J.; Stevenson, P. C.; Hillier, J. *Discuss. Faraday Soc.* **1951**, *11*, 55.
(21) Crepaldi, E. L.; Soler-Illia, G. J. d. A. A.; Grosso, D.; Cagnol, F.; Ribot, F.; Sanchez, C. *J. Am. Chem. Soc.* **2003**, *125*, 9770.
(22) Grosso, D.; Balkenende, A. R.; Albouy, P. A.; Ayral, A.; Amenitsch, H.; Babonneau, F. *Chem. Mater.* **2001**, *13*, 1848.
(23) Bourgeois, A.; Brunet Bruneau, A.; Fisson, S.; Demarets, B.; Grosso, D.; Cagnol, F.; Sanchez, C.; Rivory, J. *Thin Solid Films* **2004**, *447−448*, 46.
(24) Okamoto, T.; Yamaguchi, I.; Kobayashi, T. *Opt. Lett.* **2000**, *25*, 372.
(25) Ye, J.; Bonroy, K.; Nelis, D.; Frederix, F.; D'Haen, J.; Maes, G.; Borghs, G. *Colloids Surf., A* **2008**, *321*, 313.
(26) Burgin, J.; Liu, M.; Guyot-Sionnest, P. *J. Phys. Chem. C* **2008**, *112*, 19279–19282.
(27) Pastoriza-Santos, I.; Sánchez-Iglesias, A.; García de Abajo, F. J.; Liz Marzán, L. M. *Adv. Funct. Mater.* **2007**, *17*, 1443.
(28) Kim, K. S.; Barteau, M. A. *J. Mol. Catal.* **1990**, *63*, 103.
(29) Diebold, U. *Surf. Sci. Rep.* **2003**, *48*, 53.

JP106528N